

1 On the validity of effective formulations for transport 2 through heterogeneous porous media

3 **J.-R. de Dreuzy^{1,2} and J. Carrera²**

4 [1] {Géosciences Rennes (UMR CNRS 6118), Campus de Beaulieu, Université de Rennes 1,
5 35042 Rennes cedex, France }

6 [2] {GHS UPC-CSIC, Institute of Environmental Analysis and Water Studies (IDAEA),
7 CSIC, Barcelona, Spain }

8 Correspondence to: J.-R. de Dreuzy (Jean-Raynald.de-Dreuzy@univ-rennes1.fr)

9 **Abstract**

10 Geological heterogeneity enhances spreading of solutes, and causes transport to be anomalous
11 (i.e., non-Fickian), with much less mixing than suggested by dispersion. This implies that
12 modeling transport requires adopting either stochastic approaches that model heterogeneity
13 explicitly or effective transport formulations that acknowledge the effects of heterogeneity. A
14 number of such formulations have been developed and tested as upscaled representations of
15 enhanced spreading. However, their ability to represent mixing has not been formally tested,
16 which is required for proper reproduction of chemical reactions and which motivates our
17 work. We propose that, for an effective transport formulation to be considered a valid
18 representation of transport through Heterogeneous Porous Media (HPM), it should honor
19 mean advection, mixing and spreading. It should also be flexible enough to be applicable to
20 real problems. We test the capacity of the Multi-Rate Mass Transfer (MRMT) to reproduce
21 mixing observed in HPM, as represented by the classical multi-Gaussian log-permeability
22 field with a Gaussian correlation pattern. Non-dispersive mixing comes from heterogeneity
23 structures in the concentration fields that are not captured by macrodispersion. These fine
24 structures limit mixing initially, but eventually enhance it. Numerical results show that,
25 relative to HPM, MRMT models display a much stronger memory of initial conditions on
26 mixing than on dispersion because of the sensitivity of the mixing state to the actual values of
27 concentration. Because MRMT does not reconstitute the local concentration structures, it induces
28 smaller non-dispersive mixing than HPM. However long-lived trapping in the immobile zones
29 may sustain the deviation from dispersive mixing over much longer times. While spreading
30 can be well captured by MRMT models, in general non-dispersive mixing cannot.

31

1 1 Introduction

2 Transport is anomalous in heterogeneous porous media. Anomalous transport observations
3 include tailing in concentration breakthrough curves and plumes, or the strong increase in the
4 rate of spreading of plumes. Several frameworks have been developed to generalize the
5 Advection Dispersion Equation (ADE) and overcome its limitations [*Fripiat and Holeyman,*
6 2008]. All these alternative frameworks share the goal to model complex permeability,
7 velocity and concentration patterns in unified parsimonious effective equations. The limited
8 number of parameters makes them efficient for the limited quantity of data usually available.
9 In fact, they can be parameterized from breakthrough curves. They comply with the broad
10 residence time distributions and non-local transport processes observed in reality [*Gjetvaj et*
11 *al.*, 2015; *Le Borgne and Gouze*, 2008; *Willmann et al.*, 2008]. They represent the
12 consequences of complex concentration patterns, of simultaneous concentration trapping and
13 fast progress on residence times while averaging out all the fine concentration structures in
14 the upscaling process. These anomalous transport frameworks have proven to be highly
15 effective for residence times, transport time distribution and effective spreading both
16 phenomenologically and practically [*Berkowitz et al.*, 2006; *Neuman and Tartakovsky*, 2009].
17 However, their ability to reproduce mixing, which is required for properly reproducing
18 chemical reactions, has not been tested.

19 We argue that an effective transport formulation should honor not only the mean advection,
20 and spreading observed in Heterogeneous Porous Media (HPM), but also the evolution of
21 mixing. This should not be understood as limiting anomalous transport frameworks but at
22 extending them to handle broader ranges of physical and chemical processes, and at further
23 promoting the approach of effective equations that upscale out the fine scale structures to
24 retain only their main consequences in terms of transport, reactivity and reactive transport
25 couplings.

26 Here, we investigate the relevance of Multi-Rate Mass Transfer (MRMT) framework to
27 model not only spreading but also mixing. MRMT is taken as a typical anomalous transport
28 framework. Its advantage lies in providing local concentrations, which can be
29 straightforwardly used to evaluate concentration variance, mixing and mixing induced
30 reactivity [*Babey et al.*, 2014; *Carrera et al.*, 1998; *de Dreuzy et al.*, 2013; *Haggerty and*
31 *Gorelick*, 1995], as well as the apparent reduction in the rate of kinetic reactions [*Dentz et al.*,
32 2011]. The question is whether its validity as a representation of transport through

1 heterogeneous porous media (HPM) can be extended to reproduce the effects of the evolution
2 of mixing rates resulting from the stretching and folding associated to complex velocity
3 structures [*de Anna et al.*, 2014b; *Jimenez-Martinez et al.*, 2015; *Le Borgne et al.*, 2015].

4 This comparison is especially appropriate as anomalous transport processes are currently
5 extended to simulate reactive transport processes [*Cirpka and Valocchi*, 2007; *Clement*, 2001;
6 *de Barros et al.*, 2012; *Donado et al.*, 2009; *Hochstetler et al.*, 2013; *Luo et al.*, 2008; *Luo*
7 *and Cirpka*, 2011; *Orgogozo et al.*, 2013; *Schneider et al.*, 2013]. They deal with chemical
8 reactivity either in a stochastic manner, representing reactivity with molecular analogies, or in
9 classical approaches by means of concentrations [*Bolster et al.*, 2010; *Cirpka et al.*, 2012;
10 *Ding et al.*, 2013; *Hayek et al.*, 2012; *Knutson et al.*, 2007; *Zhang et al.*, 2013]. Extensions are
11 both required for applications purposes and attractive for capturing the consequences of
12 anomalous transport to potential "anomalous" and enhanced reactivity [*Battiato et al.*, 2009;
13 *Sadhukhan et al.*, 2014; *Scheibe et al.*, 2015; *Tartakovsky et al.*, 2009].

14 Some assessment of MRMT to model reactivity in HPM has been made in former works
15 [*Willmann et al.*, 2010]. Equivalent reactivity has been evaluated at some well-defined travel
16 distances on MRMT calibrated on residence time distributions. Here we follow a different
17 avenue by analyzing the temporal development of spreading and mixing. We extend the
18 integrated assessment of mixing-induced reactivity at given travel distances to its temporal
19 development.

20 Our contribution concerns the comparison of different models much more than the HPM and
21 MRMT model themselves. For the sake of completeness, we recall model equations and
22 simulation methods in section 2 (models and methods) and measures of spreading and mixing
23 in section 3. We use these measures to propose the conditions that should be met by effective
24 (upscaled) transport formulations to be considered valid representations of transport through
25 heterogeneous porous media (Section 4). We then test whether MRMT formulations meet the
26 proposed conditions (Section 5). While this last section depends on the specific choice of the
27 MRMT framework as an equivalent transport model, the comparison methodology is
28 independent of it and can be used to assess transport equations respecting both spreading and
29 mixing.

2 Model and Methods

We present sequentially the Multi-Rate Mass Transfer (MRMT) and Heterogeneous Porous Media (HPM) models. As they are both well known, we present only the main equations and highlight the critical assumptions of importance in this study.

2.1 Multi-Rate Mass Transfer model (MRMT)

Multi-Rate Mass Transfer models express anomalous transport by the interaction between transport in a mobile zone and a series of immobile zones [Carrera *et al.*, 1998; Haggerty and Gorelick, 1995]. Transport in the mobile zone is advective and dispersive with a mean solute velocity v (water flux divided by mobile porosity, ϕ) and a dispersion coefficient d . Each immobile zone i is parameterized by a characteristic rate α_i (inverse of a characteristic exchange time) and an immobile porosity ϕ_i . The concentrations c and c_i ($i=1..N$) in the mobile and immobile zones, respectively, are determined by the following set of equations:

$$\phi \frac{\partial c}{\partial t} + \sum_{i=1}^N \phi_i \frac{\partial s_i}{\partial t} = -q \frac{\partial c}{\partial x} + d \frac{\partial^2 c}{\partial x^2}. \quad (1)$$

$$\frac{\partial c_i}{\partial t} = \alpha_i (c - c_i) \text{ for } i = 1, \dots, N \quad (2)$$

The ratio of immobile to mobile water volumes is rated by the total capacity ratio $\beta = \sum \phi_i / \phi$. The term capacity derives from the fact that MRMT formulations were originally devised to represent trapping by sorption in hard-to-reach sorption sites, which were characterized by capacity (including both dissolved and sorbed solute mass) [see, e.g., Haggerty and Gorelick, 1995]. We use here an equivalent MRMT formulation for non-sorbing solutes, so as to facilitate comparison with HPM.

Initial and boundary conditions will be described later for both MRMT and HPM models. MRMT models differ by the distributions of characteristic rates α_i and immobile porosities ϕ_i . Among the available models [Cvetkovic, 2012; Haggerty *et al.*, 2000], we choose a uniform distribution for characteristic times ($1/\alpha_i$) bounded by the two extreme rates $\alpha_1=1/t_1$ and $\alpha_N=1/t_N$ ($t_1 < t_N$) and a power-law distribution for ϕ_i :

$$\phi_i \sim \alpha_i^{m-3}. \quad (3)$$

1 The power-law distribution is consistent with observed breakthrough curves in Heterogeneous
 2 Porous Media, which often display long tails that appear linear in $\log(c)$ versus $\log(t)$ [*Gouze*
 3 *et al.*, 2008; *Haggerty et al.*, 2004; *Li et al.*, 2011; *Silva et al.*, 2009; *Willmann et al.*, 2008].
 4 This tailing is well modeled by a power law, such that the breakthrough concentration c
 5 evolves as $c \sim t^m$. *Haggerty et al.* (2000) showed that the slope m relates to the exponent of the
 6 power-law distribution of the MRMT rates (equation (3)). m is generally found to be in the
 7 interval [1.5;2.5] but little is known about its relationship to the geological heterogeneity.
 8 *Willmann et al.* (2008) found some correlation between the degree of connectivity and the
 9 slope. The more connected the field, the smaller the slope. In this context, fracture/matrix
 10 exchanges in fractured media represent the lowest bound ($m=1.5$), which is controlled by
 11 diffusion into immobile regions [*Haggerty and Gorelick*, 1995]. On the contrary, a slope m of
 12 2.5 may represent a heterogeneous but poorly connected hydraulic conductivity field, where
 13 late time arrival is controlled by slow advection.

14 We simulate MRMT models with a standard time- and space-adaptative method that
 15 preserves mass [*de Dreuzy et al.*, 2013] and always complies with the CFL conditions [*Daus*
 16 *et al.*, 1985]. The advective and the diffusive processes in the mobile zone as well as the
 17 exchange with the immobile zones are treated with a sequential non-iterative coupling
 18 method. These methods lead to efficient simulations of large spatial domains and extended
 19 times with initial refined resolutions. We have successfully compared them with a more
 20 classical fixed-time Galerkin finite element methods integrated with the 4th order Runge-Kutta
 21 method (ode45 function of Matlab) and found relative differences less than 10^{-3} %.
 22 Simulations have been performed over the time required for transport to reach its asymptotic
 23 regime.

24 **2.2 Heterogeneous Porous Media (HPM)**

25 For reference purposes, we restrict the analysis to heterogeneity of hydraulic conductivity (K)
 26 as represented by the classical 2D Gaussian correlated multi-Gaussian log- K fields. These are
 27 characterized by their isotropic correlation function:

28

$$C(r) = \sigma_Y^2 \exp\left(-\left(\frac{r}{\lambda}\right)^2\right) \quad (4)$$

1 with r the distance, λ the correlation length, which is used to scale distances, and σ_Y^2 the
2 variance of the logarithm of $Y=\log-K$. We use simulation results performed in previous studies
3 [*de Dreuzy et al.*, 2012] obtained on 2D domains of sizes L_L and L_T in the direction parallel
4 and orthogonal, respectively, to the mean flux. L_L is large enough to avoid any finite-size
5 effects (from 10^2 to 10^3 correlation lengths λ). Boundary conditions for flow and transport are
6 periodic in the transverse direction to minimize boundary effects. L_T is of the order of 100
7 times λ to ensure initially ergodic transport conditions. Under such uniform extended injection
8 conditions, transport in HPM can be considered ergodic and can be fundamentally compared
9 with a 1D MRMT model. The immobile zones of MRMT can be viewed as representing the
10 low velocity zones of HPM, so that the mobile zone may represent the high velocity channels.
11 Flow is solved with a finite volume scheme with permeameter-like boundary conditions under
12 a unit head gradient. Transport is simulated using the ADE, with heterogeneous advection and
13 homogeneous diffusion. Therefore, it is characterized by the Peclet number Pe equal to the
14 mean velocity times the correlation length divided by the diffusion coefficient. Transport is
15 simulated with a random walk Lagrangian method. Numerical methods are exhaustively
16 described in several previous papers [*Beaudoin et al.*, 2006; *Beaudoin et al.*, 2007; *Beaudoin*
17 *et al.*, 2011].

18 **2.3 Injection and boundary conditions**

19 The same type of injection and boundary conditions are used for both models. Flow has a
20 major flow direction imposed in HPM by a head gradient in the longitudinal direction and
21 periodic boundary direction in the transverse direction. For transport, reflecting and absorbing
22 boundary conditions are used respectively upstream and downstream [*Beaudoin and de*
23 *Dreuzy*, 2013]. Injection is performed downstream to the inlet boundary to minimize
24 boundary effects.

25 Extended injection conditions are used for the HPM and MRMT models. Concentrations are
26 homogeneous orthogonally to the main flow direction within a square wave of longitudinal
27 and transverse widths ΔL_0 and ΔT_0 , respectively. In the HPM case, concentration is a sole
28 function of the coordinate x_L along the flow direction:

$$c(\mathbf{x}, t = 0) = c_0(x_L) \quad (5)$$

29 with c_0 given by:

$$c_0(x) = \begin{cases} \frac{m_0}{\phi_T \Delta T_0 \Delta L_0} & \text{if } x_0 < x < x_0 + \Delta L_0 \\ 0 & \text{otherwise} \end{cases} \quad (6)$$

1 ϕ_T is the total porosity. To ensure that the same mass m_0 is injected in the HPM and MRMT
 2 cases, we adapt the initial state of the MRMT model to:

$$c(x, t = 0) = c_i(x, t = 0) = c_0(x) \text{ for } i = 1..N. \quad (7)$$

3 Spreading becomes independent of the injection length when the longitudinal plume size
 4 becomes significantly larger than ΔL_0 . Mixing depends more critically than spreading on the
 5 injection conditions, as the initial concentration value depends on the injection width ΔL_0
 6 (equation (6)).

7 **3 Measures of spreading and mixing**

8 **3.1 Spreading**

9 For an extended plume, spreading is generally measured by the square root of the second
 10 centered moment of the spatial distribution of concentration σ_L :

$$\sigma_L(t) = \sqrt{m_L^{(2)}(t) - m_L^{(1)}(t)^2} \quad (8)$$

11 where $m_L^{(k)}(t)$ is the k-th order moment of the concentration distribution

$$m_L^{(k)}(t) = \int_{\Omega} x_L^k c(\mathbf{x}, t) d^d x / \int_{\Omega} c(\mathbf{x}, t) d^d x \quad (9)$$

12 with x_L the coordinate of \mathbf{x} in the direction parallel to the main flow direction (longitudinal
 13 direction) and Ω the flow domain. With this definition, σ_L can be viewed as the longitudinal
 14 extent of the plume (i.e., how far it spreads). Dispersion is the rate of spreading (i.e., time
 15 derivative of σ_L^2), usually characterized by the longitudinal dispersivity α_L :

$$\alpha_L = \frac{1}{2v} \frac{d\sigma_L^2}{dt} \quad (10)$$

16 where v is the plume velocity equal to the time derivative of the mean position plume $m_L^{(1)}(t)$.
 17 α_L increases until it converges to an asymptotic value α_{LA} , thus defining in turn the
 18 asymptotic regime [Dagan, 1990; Gelhar, 1993].

1 In MRMT, spreading comes from the exchanges to the mobile zone. That is, spreading results
 2 from trapping. Solutes are slowed down and dispersed by the exchanges with the immobile
 3 zones. The resulting dispersivity is a monotonously increasing function of the residence times
 4 in immobile zones (both their mean $\langle \tau_{MRMT} \rangle$ and range $(t_N - t_1)$). The dispersivity induced by
 5 the dispersive and diffusive processes in the mobile zone is comparatively negligible and
 6 could be disregarded.

7 In HPM, spreading comes both from diffusive exchanges with low velocity zones and from
 8 spatial fluctuations of the velocity field [*de Dreuzy et al., 2007; Salandin and Fiorotto, 1998*].
 9 The asymptotic dispersivity increases both with the correlation length λ and with the log-K
 10 variance σ_Y^2 :

$$\alpha_{LA}(HPM) = \lambda g(\sigma_Y^2) h(\sigma_Y^2, Pe) \quad (11)$$

11 where g is either a linear function for small values of σ_Y^2 ($\sigma_Y^2 < 1$) and a quadratic function at
 12 larger values [*de Dreuzy et al., 2007*]. $h(\sigma_Y^2, Pe)$ is a correction factor accounting for diffusion
 13 [*Beaudoin et al., 2010*]. Local diffusion reduces the effective dispersivity in the high
 14 heterogeneity cases by releasing solutes from the low velocity zone and truncating the
 15 trapping times induced by slow advection.

16 Any concentration plume can be approximated by a Gaussian concentration profile $c_D(\mathbf{x}, t)$,
 17 defined by the two first moments, $m_L^{(1)}(t)$ as mean and $\sigma_L^2(t)$ as variance. It is the smoothest
 18 equivalent profile. Both MRMT and HPM converge asymptotically to this profile. However,
 19 it is far away from the full concentration profile $c(\mathbf{x}, t)$ at any time as shown by the comparison
 20 of Figure 1. At early times (left snapshots on Figure 1), the concentration profile remains
 21 heterogeneous especially in the transverse direction with both higher and lower
 22 concentrations. Around the advection time, defined as the correlation length λ divided by the
 23 plume velocity v , the deviation reaches its maximum. At this point, the Gaussian
 24 concentration profile has become much more diluted than the real concentration field (second
 25 from the left snapshot of Figure 1). Concentration inhomogeneities decrease very slowly and
 26 remain over very long times even though the range of concentration values decreases (two
 27 right-most snapshots of Figure 1) [*de Anna et al., 2014a; Jimenez-Martinez et al., 2015; Le*
 28 *Borgne et al., 2011*].

1 In summary, in HPM, dispersivity comes primarily from the velocity structure, which drives
 2 the generation of gradients in concentration and thus mixing. Instead, in MRMT, effective
 3 dispersivity is controlled by mobile-immobile exchanges and delays the actual mixing
 4 between the immobile and mobile solute concentrations.

5 **3.2 Mixing**

6 The Gaussian profile only gives a crude approximation of the concentration field with a
 7 strong deviation on the distribution of concentration values, especially at early times when
 8 diffusion has not homogenized the concentration field in the transverse direction (Figure 1).
 9 Actual concentrations remain much higher and closer to the initial concentration value than in
 10 the Gaussian profile prediction. That is the initial concentrations are much less diluted (i.e.,
 11 mixed) than in the maximum entropy Gaussian distribution. The Gaussian profile $c_D(\mathbf{x},t)$ thus
 12 sets a lower bound to the effective concentration variability. Therefore, it is most natural to
 13 compare the actual distribution of concentration values to that of the Gaussian profile in order
 14 to describe the mixing state. Notice that, contrary to spreading, we are not concerned here
 15 with the spatial distribution, but only with the values of concentration and their time
 16 evolution, which are most simply characterized by the second moment. We quantified the
 17 deviation from the Gaussian mixing regime as the ratio of the actual concentration second
 18 moment $M(t)$ to the second moment $M_D(t)$ of the Gaussian profile concentration $c_D(\mathbf{x},t)$ minus
 19 1 [*de Dreuzy et al.*, 2012]:

$$\gamma(t) = \frac{M(t)}{M_D(t)} - 1. \quad (12)$$

20 with

$$M(t) = \int_{\Omega} c^2 d^d x \quad (13)$$

21 and the second moment of the reference Gaussian concentration:

$$M_D(t) = \frac{m_0^2}{2\sqrt{\pi\Delta T_0}\sigma_L}. \quad (14)$$

22 M_D is directly the square of the injected mass m_0^2 divided by an effective area occupied by
 23 the plume $2\sqrt{\pi\Delta T_0}\sigma_L$. As $M(t)$ is always larger than $M_D(t)$, γ is always positive. γ is initially
 24 and asymptotically very close to zero. It is however significantly positive while the

1 concentration distribution is far from the Gaussian profile. $M(t)$, which we have introduced
 2 here as a measure of global concentration variability, is a widely used measure, as its time
 3 derivative, dissipation rate, determines the physical constrains of chemical reactivity [*de*
 4 *Simoni et al.*, 2005; *Le Borgne et al.*, 2010]. The dissipation is also closely related to the
 5 dilution index, which is another measure of mixing [*Kitanidis*, 1994; *Rolle et al.*, 2009]. It
 6 should be finally noticed that γ and M_D fully characterize the mixing state given by M :

$$M = M_D (1 + \gamma). \quad (15)$$

7 In HPM models, resistance to dispersive mixing, as we can also call γ , is enhanced by
 8 heterogeneity and reduced by large diffusion rates (smaller Peclet number) [*de Dreuzy et al.*,
 9 2012]. γ sharply increases at initial times to a maximum value γ_{\max} , at a time $t_{\gamma_{\max}}$ close to the
 10 advection time, and slowly decreases back to 0 (Figure 2). The time range over which γ is
 11 significantly non zero can be characterized by r_{γ} , which is the ratio of the upper and lower
 12 times at which γ is equal to a quarter of its maximal value γ_{\max} . While the amplitude of γ
 13 depends on the variability of the velocities and on the rate of advection to diffusion, the shape
 14 of the function γ remains unchanged by the K field heterogeneity (σ_Y^2), the ratio of advection
 15 to diffusion (Pe), and the width of the initial conditions (ΔL_0). The time range r_{γ} over which γ
 16 is non-negligible also remains constant (Figure 2). Therefore, $t_{\gamma_{\max}}$ can be used for scaling
 17 time, so that γ can be written as:

$$\gamma(t) = \gamma_{\max} f\left(\frac{t}{t_{\gamma_{\max}}}\right) \quad (16)$$

18 where f is the characteristic scaling function (Figure 2, insert). A similar constant shape
 19 behavior has been noted for viscous fingering in heterogeneous velocity fields [*Jha et al.*,
 20 2011a; b].

21 **4 Conditions for effective formalisms of transport through HPM**

22 We propose four conditions for any effective transport formulation to be considered as a valid
 23 representation of transport through heterogeneous media. In essence, an effective transport
 24 equation should yield the same mean advection, spreading and mixing as the HPM and be
 25 sufficiently flexible to represent real problems. Evaluation of these conditions can be done as
 26 follows:

1 (1) **Mean advection** simply requires mean water velocity (i.e., mean plume velocity for non-
 2 reactive solutes) to equal $v = q / \phi_r$. This condition can be met by all published upscaled
 3 transport equations, by imposing some simple constraints on their parameters. In MRMT, it is
 4 sufficient to impose $\phi_r = \phi + \sum \phi_i = \phi(1 + \beta)$.

5 (2) **Spreading** is characterized by dispersivity, which measures the rate of growth of plume
 6 size (equation (10)). In cases where asymptotic dispersion is reached, this condition implies
 7 that dispersivity of the effective equation should tend to the asymptotic dispersivity of the
 8 HPM. Otherwise, dispersion (or directly, spread, as measured by σ_L) can be compared for a
 9 spatial scale comparable to the problem dimension (e.g., size of the aquifer, or distance
 10 covered by the plume).

11 In addition, the time required to reach the above dispersion value should also be honored by
 12 the effective formulation to ensure that the rate of growth of the plume is reproduced. In our
 13 case, where asymptotic dispersion is reached, we propose to define this criterion in terms of
 14 r_α , mean distance covered by the plume at the time $t_{\alpha_{LA}/2}$ where dispersivity reaches half of
 15 its asymptotic value normalized by the asymptotic dispersivity α_{LA} :

$$r_\alpha = \frac{v t_{\alpha_{LA}/2}}{\alpha_{LA}} \quad (17)$$

16 where $t_{\alpha_{LA}/2}$ is implicitly defined by

$$\alpha(t_{\alpha_{LA}/2}) = \frac{\alpha_{LA}}{2}. \quad (18)$$

17 r_α can also be interpreted as the ratio of advective and dispersive scales like in the definition
 18 of the Peclet number.

19 (3) **Mixing** is required for properly reproducing fast reactions (slow reactions should be
 20 properly reproduced if the resident time distribution is honored, which is assured if mean
 21 advection and dispersion are reproduced). As discussed above, mixing is essentially
 22 dispersive and well characterized by M_D (equation (14)) for late times. Therefore, assuming
 23 dispersion to be well reproduced, an effective transport formulation only needs to reproduce
 24 the deviation from dispersive mixing, characterized by γ (equation (12)). In a first stage, the
 25 comparison can be restricted to the amplitude of the deviation γ_{\max} and the time range over

1 which it extends r_{γ} . In a more advanced stage, the characteristic shape of the γ function, f , can
2 be used for comparison.

3 To compare the timings of spreading and mixing, we define the additional criterion r_{MT} as the
4 ratio of the characteristic spreading time $t_{\alpha_{LA}/2}$ to the characteristic mixing time $t_{\gamma_{max}}$

$$r_{MT} = \frac{t_{\gamma_{max}}}{t_{\alpha_{LA}/2}}. \quad (19)$$

5 r_{MT} compares the timing of the development of the resistance to mixing and of spreading and
6 rates the lag between the timing of mixing and spreading.

7 (4) **Flexibility.** Most of the work on effective transport is of a theoretical nature, but the
8 ultimate goal should be application to real problems. This implies that a valid transport
9 formulation should be able to accommodate different types of boundary conditions and flow
10 regimes (i.e., transient flow) and dimensions. Most importantly, it should accommodate
11 characterization. Dispersion usually includes the effects of heterogeneity and uncertainty.
12 Whereas the latter is reduced by aquifer characterization, the former is not. Specifically,
13 hydrologists use geology, hydraulics, geophysics, hydrochemistry and isotopes to figure out,
14 among other things, the patterns of spatial variability of hydraulic conductivity. The resulting
15 models display variability not only in the mean log- K but also on their correlation distance
16 and variance. An effective transport formulation should be able to honor this variability.

17 **5 Results and discussion**

18 We consider well established that MRMT, and other non-local in time formulations, can
19 reproduce mean advection and spreading, as discussed in the introduction. Mean advection in
20 the MRMT approach is equivalent to that of the HPM provided that flux and total porosity are
21 equivalent. And the distribution of residence times in immobile zones can be adapted so that
22 the asymptotic dispersivity of the MRMT model be equal to that of the HPM model in
23 equation (11). It is always possible as dispersivity is an increasing function of the residence
24 times. This imposes a condition on the temporal range of t_1, \dots, t_N or equivalently on their mean
25 residence time $\langle \tau_{MRMT} \rangle$. As trapping in the immobile zones is the main dispersive mechanism,
26 the mean residence time is logically adapted to calibrate the asymptotic dispersivity. With the
27 total flow imposed to be set by the HPM, the characteristic spatial scale is the typical plume
28 position at $\langle \tau_{MRMT} \rangle$. As the characteristic spatial and temporal scales are interrelated to ensure

1 consistent asymptotic behaviors, comparison of results can be performed on dimensionless
2 terms and should ensure consistent preasymptotic regimes. In fact, MRMT are calibrated on
3 tracer tests and breakthrough information, but this does not ensure a good reproduction of
4 mixing [Luo and Cirpka, 2011]. Therefore, we restrict our comparison to mixing criteria and
5 sensitivity to initial conditions.

6 **5.1 Comparison of mixing in HPM and MRMT**

7 In Heterogeneous Porous Media (HPM), the temporal extension of the deviation from the
8 dispersive mixing regime $r_{t\gamma}$ does not depend significantly on the permeability heterogeneity,
9 as also expressed by the constancy of the shape of γ (Figure 2). We thus compare the shape of
10 γ obtained for the HPM with $\sigma_Y^2=9$ (f function of equation (16)) to shapes of γ obtained for
11 various MRMT models obtained under consistent injection conditions (equations (6) and (7)).
12 For MRMT, extreme values have been investigated to get the possible range of behaviors. For
13 slopes m , we adopted the range observed in nature as discussed in section 2.1 with m varying
14 between $m=1.5$ (typical fracture/matrix case) and $m=2.5$. The Single Rate Mass Transfer
15 (SRMT) is also shown for comparison. The porosity ratio β does not have an upper bound. In
16 fact, ideally, the mobile porosity could be zero. We adopted $\beta=150$ as a large upper value.
17 Larger upper values would not affect results and might cause numerical difficulties. The same
18 can be said for t_N/t_1 for which we took $t_N/t_1=10^3$ as the upper bound. The analysis presented
19 hereafter has been made for different combination of parameters within these bounds. As all
20 models lead to consistent conclusions, we only present the most characteristic results.

21 All MRMT models capture the sharp rise of γ at times smaller than $t_{\gamma\max}$ (Figure 3). The sharp
22 rise comes from a strong initial divergence from the equivalent Gaussian concentration
23 profile. Initial behavior is dominated by the contrast of the quickly progressing concentrations
24 in the mobile zones and trailing concentrations in the low flow or immobile zones. On one
25 hand, dispersion induces a sharp decrease of M_D , which is inversely proportional to σ_L
26 (equation (14)). On the other hand, trapping maintains high concentrations in the immobile
27 zone and high values for the second moment of the concentration distribution M . Divergence
28 of M from M_D increases until it reaches its maximum at $t_{\gamma\max}$.

29 At larger times, progressive release of solute mass from the immobile zone and equilibration
30 with the concentration values in the mobile zone let f decrease. The insert of Figure 3
31 highlights in a lin-lin graph the differences of the decrease stage. The MRMT model that best

1 matches the scaling function f is obtained for $m=2.25$. For power law slopes m larger than 2,
2 the decrease of f is qualitatively similar to that of the single-rate mass transfer model. For m
3 values closer to 2, the deviation is more sustained but displays the same decreasing trend. The
4 behavior changes significantly when m becomes smaller than 2, with a very slow decrease of f
5 coming directly from the effect of the slow drainage of the immobile zones having the
6 smallest rates (long exchange times). At least in MRMT models with m lower than 2, trapping
7 displays a much longer memory effect in MRMT than in HPM.

8 While similar to HPM for the extension of the non-dispersive mixing regime, MRMT models
9 with slopes m larger than 2 converge to less anomalous Single Rate Mass Transfer. In terms
10 of mixing, this translates in small amplitudes in γ (small γ_{\max} values). For $m=2.25$ and
11 $\Delta L_0 / \alpha_{LA} = 0.075$, we have computed γ_{\max} for a large variety of t_N/t_1 and β values, the only
12 two remaining parameters of the MRMT model. γ_{\max} first increases with t_N/t_1 and β and
13 quickly saturates to a maximal value of 2.85 (Table 1). γ_{\max} varies between 0.57 and 2.85 by a
14 maximum factor of 5. In the HPM case, however, γ_{\max} is always larger than 3, reaches values
15 of 15 for a Peclet number Pe of 100, scales like the square root of Pe and is thus not limited in
16 amplitude.

17 MRMT models cannot match both the amplitude and the timing of γ . For MRMT models with
18 m -slopes larger than 2, mixing is far more dispersive in MRMT than in HPM (smaller
19 deviation values γ in the MRMT models). MRMT models with m -slopes smaller than 2
20 induce larger but much too sustainable deviations. As a result, MRMT models have a stronger
21 memory of trapping or display less non dispersive-mixing, without excluding to display both
22 differences simultaneously. The difficulties of MRMT models to capture mixing might be
23 linked to the existence of the structure of concentrations in lamellas where stretching and
24 folding extends the concentration front and enhance the eventual mixing by diffusion (Figure
25 1) [de Anna et al., 2014b; Le Borgne et al., 2015].

26 Concerning the non-dispersive mixing shapes of the scaled function f , MRMT models display
27 a much broader range of shapes than HPM. The invariant shape property of HPM is not
28 recovered in MRMT. On the contrary, MRMT shapes depend strongly on the distribution of
29 transfer rates. This is an advantage to match a wider range of cases issuing possibly different γ
30 functions. But it is a drawback to fit just one case as it restricts the MRMT models that can
31 match HPM simulations with broad ranges of Pe and σ_Y^2 values.

1 5.2 Influence of initial injection size

2 To qualify the memory effect in MRMT and HPM, we analyze their sensitivity to the initial
3 injection width ΔL_0 . Spreading as defined by the characteristic longitudinal plume extension
4 (equations (8), (9) and (10)) does not depend on the initial concentration c_0 (equation (6)). σ_L
5 is initially of the order of ΔL_0 and quickly becomes larger. Spreading loses quickly any
6 memory of the initial conditions. We note that this is the case because sampling effects do not
7 intervene as the transverse injection scale is assumed large enough to ensure by itself ergodic
8 sampling. Like spreading, the second moment of the reference Gaussian concentration $M_D(t)$
9 does not depend either on the initial concentration but only on the injected mass divided by
10 the characteristic area occupied by the plume ($\Delta T_0 \sigma_L$) (equation (14)).

11 The concentration second moment $M(t)$ (equation (13)) however depends critically on the
12 injection width through the relation between injected mass and concentration (equation (6)).
13 At initial times, the concentration second moment is proportional to the injected concentration
14 value. At late times, the concentration second moment has lost the memory of the initial
15 concentration and is only function of the injected mass m_0 . As a result, we expect that the
16 concentration second moment and the deviation towards the dispersive mixing regime γ
17 depends on the injection conditions, here represented by the injection width ΔL_0 . On the basis
18 of numerical simulations, we compare the evolution of γ with ΔL_0 for HPM and MRMT
19 models.

20 Results of the γ function for both MRMT and HPM models are displayed on Figure 4a and
21 Figure 4b, respectively, for different injection sizes. We have performed simulations for
22 comparable ranges of $\Delta L_0/\alpha_{LA}$ values (0.005-0.1 for HPM and 0.02-0.4 for MRMT). We have
23 checked numerically that the results displayed for the two specific displayed MRMT and
24 HPM cases display generic tendencies. In both models, injection width has a critical influence
25 on γ (Figure 4). Smaller injection windows let the initial concentration increase and enhance
26 the deviation towards the dispersive mixing regime. We use the maximum deviation γ_{\max} to
27 characterize the overall influence of ΔL_0 . In the MRMT and HPM models, maximum
28 deviations γ_{\max} have different scaling (Figure 4a and b, inserts):

$$\begin{aligned} \gamma_{\max} &\sim (\Delta L_0)^{-1} \text{ for MRMT} \\ \gamma_{\max} &\sim (\Delta L_0)^{-0.5} \text{ for HPM} \end{aligned} \quad (20)$$

1 For MRMT, γ_{\max} evolves like the initial concentration level (equations (6) and (7)). For HPM,
2 γ_{\max} has the same scaling for the initial conditions $\gamma_{\max} \sim 1/\sqrt{\Delta L_0}$ and for the diffusion
3 coefficient as $\gamma_{\max} \sim \sqrt{Pe}$ [de Dreuzy *et al.*, 2012]. Doubling the injection width has a
4 comparable effect to doubling the diffusion coefficient. Initial dilution over ΔL_0 and dilution
5 induced by diffusive/dispersive processes reduce the overall deviation to the dispersive
6 mixing regime γ in the same proportion. The reduction of concentration in HPM comes from
7 the diffusive/dispersive processes while, in MRMT, it comes from the progressive release of
8 solutes with high concentrations close to c_0 trapped in the immobile zone. Because of their
9 differing signatures, both processes cannot be compared and the dispersive/diffusive
10 processes of HPM cannot be modeled as trapping/release mechanisms.

11 **6 Conclusion**

12 We propose conditions to test anomalous transport frameworks not only on spreading, but
13 also on mixing. We define a minimum set of 6 essential constrains that they should respect in
14 order to retain the main transport, reactivity and reactive transport couplings. These constrains
15 involve the conservation of (1) the mean advection, (2) dispersivity amplitude and (3) timing
16 generally imposed. Beyond these flow and spreading metrics, (4) amplitude and (5) timing of
17 the deviation towards the dispersive mixing regime should be respected. The last condition
18 concerns (6) the respective timings for mixing and spreading. Under ergodic injection
19 conditions, spreading is characterized by the standard dispersivity describing the evolution of
20 the plume size along the main flow direction. Mixing is characterized by the deviation from
21 the dispersive mixing regime γ defined as the second moment of the concentration distribution
22 of a conservative tracer divided by the one of a Gaussian concentration pattern with the same
23 spread minus 1 (equation (12)). Zero initially and asymptotically, γ traduces the macroscopic
24 effect on mixing of the concentration structures within the solute plume.

25 We use these criteria to evaluate Multi-Rate Mass Transfer models by comparison to
26 advective-diffusive transport simulations through Heterogeneous Porous Media (HPM)
27 represented by the classical isotropic 2D Gaussian correlated multi-Gaussian log-permeability
28 fields characterized by variances between 1 and 9. A broad range of Multi-Rate Mass Transfer
29 models (MRMT) are considered. We conclude that MRMT models cannot match both the
30 amplitude and the timing of γ . MRMT models can reproduce observed spreading rates and
31 some non-dispersive mixing. But they tend to induce larger and too sustained deviations from

1 dispersive mixing. As a result, MRMT models display a longer memory but less non
2 dispersive-mixing than HPM. We attribute this divergence to the fact that MRMT represent
3 non-dispersive mixing through trapping mechanisms, whereas it is controlled by stretching
4 and folding in HPM. Divergent sensitivities to initial conditions confirm that dispersive-
5 diffusive induced mixing in HPM cannot be modeled by mobile/immobile models.

6 Our study does not preclude however the existence of effective transport equations consistent
7 with spreading and mixing of HPM. But we argue that the proposed criteria and existing
8 results of HPM should be used as guidelines to set up effective transport equations that
9 respect spreading, mixing, and eventually reactive transport.

10 **Acknowledgements**

11 The European Union is acknowledged for its funding through the Marie-Curie fellowship
12 PIEF-GA-2009-251710 and through the project FP7-ENERGY-2012-1-2STAGE TRUST
13 (High resolution monitoring, real time visualization and reliable modeling of highly
14 controlled, intermediate and up-scalable size pilot injection tests of underground storage of
15 CO₂). The ANR is acknowledged for its funding through its Project H2MNO4 under the No.
16 ANR-12-MONU-0012-01.

17 **References**

- 18 Babey, T., J.-R. de Dreuzy, and C. Casenave (2014), Multi-Rate Mass Transfer (MRMT)
19 models for general diffusive porosity structures, *Advances in Water Resources*, 76, 146-156,
20 10.1016/j.advwatres.2014.12.006.
- 21 Battiato, I., D. M. Tartakovsky, A. M. Tartakovsky, and T. Scheibe (2009), On breakdown of
22 macroscopic models of mixing-controlled heterogeneous reactions in porous media, *Advances*
23 *in Water Resources*, 32(11), 1664-1673, 10.1016/j.advwatres.2009.08.008.
- 24 Beaudoin, A., J. R. de Dreuzy, J. Erhel, and H. Mustapha (2006), Parallel Simulations of
25 Underground Flow in Porous and Fractured Media, in *Parallel Computing: Current and*
26 *Future Issues of High-End Computing, Volume 33 of NIC series, Verlag des*
27 *Forschungszentrums Jülich*, edited by W. E. N. G.R. Joubert, F.J. Peters, O. Plata, P. Tirado,
28 E. Zapata, pp. 399–406
- 29 Beaudoin, A., J. R. de Dreuzy, and J. Erhel (2007), An efficient parallel tracker for advection-
30 diffusion simulations in heterogeneous porous media, paper presented at Europar, 4641
31 Springer-Verlag, Berlin, Heidelberg Rennes, France, 28-31 August 2007.
- 32 Beaudoin, A., J.-R. de Dreuzy, and J. Erhel (2010), Numerical Monte Carlo analysis of the
33 influence of pore-scale dispersion on macrodispersion in 2-D heterogeneous porous media,
34 *Water Resour. Res.*, 46(12), W12537, 10.1029/2010wr009576.
- 35 Beaudoin, A., S. Huberson, and E. Rivoalen (2011), A particle method for solving Richards'
36 equation, *Comptes Rendus Mecanique*, 339(4), 257-261, 10.1016/j.crme.2011.01.005.

- 1 Beaudoin, A., and J. R. de Dreuzy (2013), Numerical assessment of 3-D macrodispersion in
2 heterogeneous porous media, *Water Resources Research*, 49(5), 2489–2496,
3 10.1002/wrcr.20206.
- 4 Berkowitz, B., A. Cortis, M. Dentz, and H. Scher (2006), Modeling non-Fickian transport in
5 geological formations as a continuous time random walk, *Reviews of Geophysics*, 44(2),
6 Rg2003, 10.1029/2005rg000178.
- 7 Bolster, D., D. A. Benson, T. Le Borgne, and M. Dentz (2010), Anomalous mixing and
8 reaction induced by superdiffusive nonlocal transport, *Physical Review E*, 82(2), 021119,
9 10.1103/PhysRevE.82.021119.
- 10 Carrera, J., X. Sánchez-Vila, I. Benet, A. Medina, G. Galarza, and J. Guimerà (1998), On
11 matrix diffusion: formulations, solution methods and qualitative effects, *Hydrogeology*
12 *Journal*, 6(1), 10.1007/s100400050143.
- 13 Cirpka, O. A., and A. J. Valocchi (2007), Two-dimensional concentration distribution for
14 mixing-controlled bioreactive transport in steady state, *Advances in Water Resources*, 30(6-
15 7), 1668-1679, 10.1016/j.advwatres.2006.05.022.
- 16 Cirpka, O. A., M. Rolle, G. Chiogna, F. P. J. de Barros, and W. Nowak (2012), Stochastic
17 evaluation of mixing-controlled steady-state plume lengths in two-dimensional heterogeneous
18 domains, *Journal of Contaminant Hydrology*, 138, 22-39, 10.1016/j.jconhyd.2012.05.007.
- 19 Clement, T. P. (2001), Generalized solution to multispecies transport equations coupled with
20 a first-order reaction network, *Water Resources Research*, 37(1), 157-163,
21 10.1029/2000wr900239.
- 22 Cvetkovic, V. (2012), A general memory function for modeling mass transfer in groundwater
23 transport, *Water Resources Research*, 48, W04528, 10.1029/2011wr011657.
- 24 Dagan, G. (1990), Transport in Heterogeneous Porous Formations: Spatial Moments,
25 Ergodicity, and Effective Dispersion, *Water Resources Research*, 26(6), 1281-1290,
26 10.1029/WR026i006p01281.
- 27 Daus, A. D., E. O. Frind, and E. A. Sudicky (1985), Comparative error analysis in finite-
28 element formulations of the advection-dispersion equation, *Advances in Water Resources*,
29 8(2), 86-95, 10.1016/0309-1708(85)90005-3.
- 30 de Anna, P., M. Dentz, A. Tartakovsky, and T. Le Borgne (2014a), The filamentary structure
31 of mixing fronts and its control on reaction kinetics in porousmedia flows, *Geophysical*
32 *Research Letters*, 41(13), 4586-4593, 10.1002/2014gl060068.
- 33 de Anna, P., J. Jimenez-Martinez, H. Tabuteau, R. Turuban, T. Le Borgne, M. Derrien, and Y.
34 Meheust (2014b), Mixing and reaction kinetics in porous media: an experimental pore scale
35 quantification, *Environmental science & technology*, 48(1), 508-516, 10.1021/es403105b.
- 36 de Barros, F. P. J., M. Dentz, J. Koch, and W. Nowak (2012), Flow topology and scalar
37 mixing in spatially heterogeneous flow fields, *Geophysical Research Letters*, 39, L08404,
38 10.1029/2012gl051302.
- 39 de Dreuzy, J.-R., A. Beaudoin, and J. Erhel (2007), Asymptotic dispersion in 2D
40 heterogeneous porous media determined by parallel numerical simulations *Water Resources*
41 *Research*, 43(W10439), 10.1029/2006WR005394.

1 de Dreuzy, J.-R., J. Carrera, M. Dentz, and T. Le Borgne (2012), Time evolution of mixing in
2 heterogeneous porous media, *Water Resources Research*, 48, W06511,
3 10.1029/2011WR011360.

4 de Dreuzy, J. R., A. Rapaport, T. Babey, and J. Harmand (2013), Influence of porosity
5 structures on mixing-induced reactivity at chemical equilibrium in mobile/immobile Multi-
6 Rate Mass Transfer (MRMT) and Multiple INteracting Continua (MINC) models, *Water*
7 *Resources Research*, 49(12), 8511-8530, 10.1002/2013wr013808.

8 de Simoni, M., J. Carrera, X. Sanchez-Vila, and A. Guadagnini (2005), A procedure for the
9 solution of multicomponent reactive transport problems, *Water Resources Research*, 41(11),
10 10.1029/2005WR004056.

11 Dentz, M., P. Gouze, and J. Carrera (2011), Effective non-local reaction kinetics for transport
12 in physically and chemically heterogeneous media, *Journal of Contaminant Hydrology*, 120-
13 21, 222-236, 10.1016/j.jconhyd.2010.06.002.

14 Ding, D., D. A. Benson, A. Paster, and D. Bolster (2013), Modeling bimolecular reactions and
15 transport in porous media via particle tracking, *Advances in Water Resources*, 53, 56-65,
16 10.1016/j.advwatres.2012.11.001.

17 Donado, L. D., X. Sanchez-Vila, M. Dentz, J. Carrera, and D. Bolster (2009),
18 Multicomponent reactive transport in multicontinuum media, *Water Resources Research*, 45,
19 10.1029/2008wr006823.

20 Frippiat, C. C., and A. E. Holeyman (2008), A comparative review of upscaling methods for
21 solute transport in heterogeneous porous media, *Journal of Hydrology*, 362(1-2), 150-176,
22 10.1016/j.jhydrol.2008.08.015.

23 Gelhar, L. W. (1993), *Stochastic Subsurface Hydrology*, Engelwood Cliffs, New Jersey.

24 Gjetvaj, F., A. Russian, P. Gouze, and M. Dentz (2015), Dual control of flow field
25 heterogeneity and immobile porosity on non-Fickian transport in Berea sandstone, *Water*
26 *Resources Research*, 10.1002/2015WR017645.

27 Gouze, P., Y. Melean, T. Le Borgne, M. Dentz, and J. Carrera (2008), Non-Fickian dispersion
28 in porous media explained by heterogeneous microscale matrix diffusion, *Water Resources*
29 *Research*, 44(11), 19, W11416, 10.1029/2007wr006690.

30 Haggerty, R., and S. M. Gorelick (1995), Multiple-rate mass transfer for modeling diffusion
31 and surface reactions in media with pore-scale heterogeneity, *Water Resources Research*,
32 31(10), 2383-2400, 10.1029/95WR10583.

33 Haggerty, R., S. A. McKenna, and L. C. Meigs (2000), On the late-time behavior of tracer test
34 breakthrough curves, *Water Resources Research*, 36(12), 3467-3479,
35 10.1029/2000WR900214.

36 Haggerty, R., C. F. Harvey, C. F. von Schwerin, and L. C. Meigs (2004), What controls the
37 apparent timescale of solute mass transfer in aquifers and soils? A comparison of
38 experimental results, *Water Resources Research*, 40(1), W01510, 10.1029/2002wr001716.

39 Hayek, M., G. Kosakowski, A. Jakob, and S. V. Churakov (2012), A class of analytical
40 solutions for multidimensional multispecies diffusive transport coupled with precipitation-
41 dissolution reactions and porosity changes, *Water Resources Research*, 48, W03525,
42 10.1029/2011wr011663.

1 Hochstetler, D. L., M. Rolle, G. Chiogna, C. M. Haberer, P. Grathwohl, and P. K. Kitanidis
2 (2013), Effects of compound-specific transverse mixing on steady-state reactive plumes:
3 Insights from pore-scale simulations and Darcy-scale experiments, *Advances in Water*
4 *Resources*, 54, 1-10, 10.1016/j.advwatres.2012.12.007.

5 Jha, B., L. Cueto-Felgueroso, and R. Juanes (2011a), Quantifying mixing in viscously
6 unstable porous media flows, *Physical review. E, Statistical, nonlinear, and soft matter*
7 *physics*, 84, 066312, 10.1103/PhysRevE.84.066312.

8 Jha, B., L. Cueto-Felgueroso, and R. Juanes (2011b), Fluid Mixing from Viscous Fingering,
9 *Physical Review Letters*, 106(19), 10.1103/PhysRevLett.106.194502.

10 Jimenez-Martinez, J., P. de Anna, H. Tabuteau, R. Turuban, T. Le Borgne, and Y. Meheust
11 (2015), Pore-scale mechanisms for the enhancement of mixing in unsaturated porous media
12 and implications for chemical reactions, *Geophysical Research Letters*, 42(13), 5316-5324,
13 10.1002/2015gl064513.

14 Kitanidis, P. K. (1994), The concept of the dilution index, *Water Resources Research*, 30(7),
15 10.1029/94WR00762.

16 Knutson, C., A. Valocchi, and C. Werth (2007), Comparison of continuum and pore-scale
17 models of nutrient biodegradation under transverse mixing conditions, *Advances in Water*
18 *Resources*, 30(6-7), 1421-1431, 10.1016/j.advwatres.2006.05.012.

19 Le Borgne, T., and P. Gouze (2008), Non-Fickian dispersion in porous media: 2. Model
20 validation from measurements at different scales, *Water Resources Research*, 44(6),
21 10.1029/2007wr006279.

22 Le Borgne, T., M. Dentz, D. Bolster, J. Carrera, J.-R. de Dreuzy, and P. Davy (2010), Non-
23 Fickian mixing: Temporal evolution of the scalar dissipation rate in heterogeneous porous
24 media, *Advances in Water Resources*, 3(12), 1468-1475, 10.1016/j.advwatres.2010.08.006.

25 Le Borgne, T., M. Dentz, P. Davy, D. Bolster, J. Carrera, J.-R. de Dreuzy, and O. Bour
26 (2011), Persistence of incomplete mixing: A key to anomalous transport, *Physical Review E*,
27 84(1), 015301, 10.1103/PhysRevE.84.015301.

28 Le Borgne, T., M. Dentz, and E. Villiermaux (2015), The lamellar description of mixing in
29 porous media, *Journal of Fluid Mechanics*, 770, 458-498, 10.1017/jfm.2015.117.

30 Li, L., H. Zhou, and J. Jaime Gomez-Hernandez (2011), Transport upscaling using multi-rate
31 mass transfer in three-dimensional highly heterogeneous porous media, *Advances in Water*
32 *Resources*, 34(4), 478-489, 10.1016/j.advwatres.2011.01.001.

33 Luo, J., M. Dentz, J. Carrera, and P. Kitanidis (2008), Effective reaction parameters for
34 mixing controlled reactions in heterogeneous media, *Water Resources Research*, 44(2),
35 W02416, 10.1029/2006wr005658.

36 Luo, J., and O. A. Cirpka (2011), How well do mean breakthrough curves predict mixing-
37 controlled reactive transport?, *Water Resources Research*, 47, W02520,
38 10.1029/2010wr009461.

39 Neuman, S. P., and D. M. Tartakovsky (2009), Perspective on theories of non-Fickian
40 transport in heterogeneous media, *Advances in Water Resources*, 32(5), 670-680,
41 10.1016/j.advwatres.2008.08.005.

- 1 Orgogozo, L., F. Golfier, M. A. Bues, M. Quintard, and T. Kone (2013), A dual-porosity
2 theory for solute transport in biofilm-coated porous media, *Advances in Water Resources*, 62,
3 266-279, 10.1016/j.advwatres.2013.09.011.
- 4 Rolle, M., C. Eberhardt, G. Chiogna, O. A. Cirpka, and P. Grathwohl (2009), Enhancement of
5 dilution and transverse reactive mixing in porous media: Experiments and model-based
6 interpretation, *Journal of Contaminant Hydrology*, 110(3-4), 130-142,
7 10.1016/j.jconhyd.2009.10.003.
- 8 Sadhukhan, S., P. Gouze, and T. Dutta (2014), A simulation study of reactive flow in 2-D
9 involving dissolution and precipitation in sedimentary rocks, *Journal of Hydrology*, 519,
10 2101-2110, 10.1016/j.jhydrol.2014.10.019.
- 11 Salandin, P., and V. Fiorotto (1998), Solute transport in highly heterogeneous aquifers, *Water*
12 *Resources Research*, 34(5), 949-961, 10.1029/98WR00219.
- 13 Scheibe, T. D., K. Schuchardt, K. Agarwal, J. Chase, X. F. Yang, B. J. Palmer, A. M.
14 Tartakovsky, T. Elsethagen, and G. Redden (2015), Hybrid multiscale simulation of a mixing-
15 controlled reaction, *Advances in Water Resources*, 83, 228-239,
16 10.1016/j.advwatres.2015.06.006.
- 17 Schneider, B., A. Paster, and D. Bolster (2013), A numerical investigation of mixing and
18 spreading across an angled discontinuity, *Advances in Water Resources*, 62, 280-291,
19 10.1016/j.advwatres.2013.09.003.
- 20 Silva, O., J. Carrera, M. Dentz, S. Kumar, A. Alcolea, and M. Willmann (2009), A general
21 real-time formulation for multi-rate mass transfer problems, *Hydrol. Earth Syst. Sci.*, 13(8),
22 1399-1411, 10.5194/hess-13-1399-2009.
- 23 Tartakovsky, A. M., G. D. Tartakovsky, and T. D. Scheibe (2009), Effects of incomplete
24 mixing on multicomponent reactive transport, *Advances in Water Resources*, 32(11), 1674-
25 1679, 10.1016/j.advwatres.2009.08.012.
- 26 Willmann, M., J. Carrera, and X. Sanchez-Vila (2008), Transport upscaling in heterogeneous
27 aquifers: What physical parameters control memory functions?, *Water Resources Research*,
28 44(12), 10.1029/2007wr006531.
- 29 Willmann, M., J. Carrera, X. Sanchez-Vila, O. Silva, and M. Dentz (2010), Coupling of mass
30 transfer and reactive transport for nonlinear reactions in heterogeneous media, *Water*
31 *Resources Research*, 46, 15, W07512, 10.1029/2009wr007739.
- 32 Zhang, Y., C. Papelis, P. Sun, and Z. Yu (2013), Evaluation and linking of effective
33 parameters in particle-based models and continuum models for mixing-limited bimolecular
34 reactions, *Water Resources Research*, 49(8), 4845-4865, 10.1002/wrcr.20368.

35

36

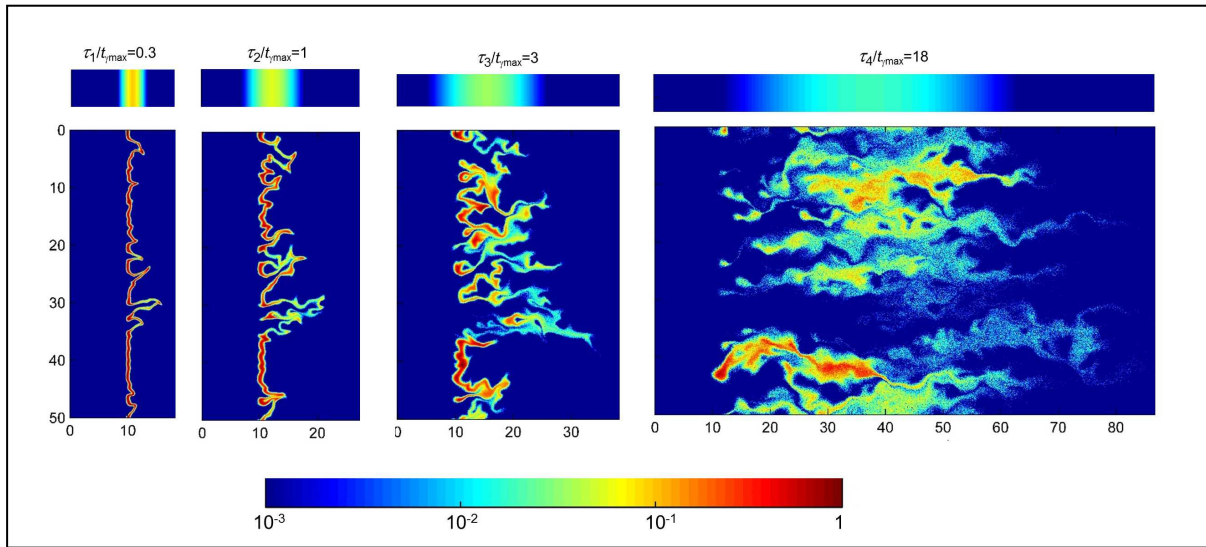
1 **Tables**

2

$t_N/t_1=100$		$\beta=100$	
β	γ_{\max}	t_N/t_1	γ_{\max}
1	0.57	1	1.47
10	1.96	10	2.72
100	2.84	100	2.84
300	2.85	694	2.74

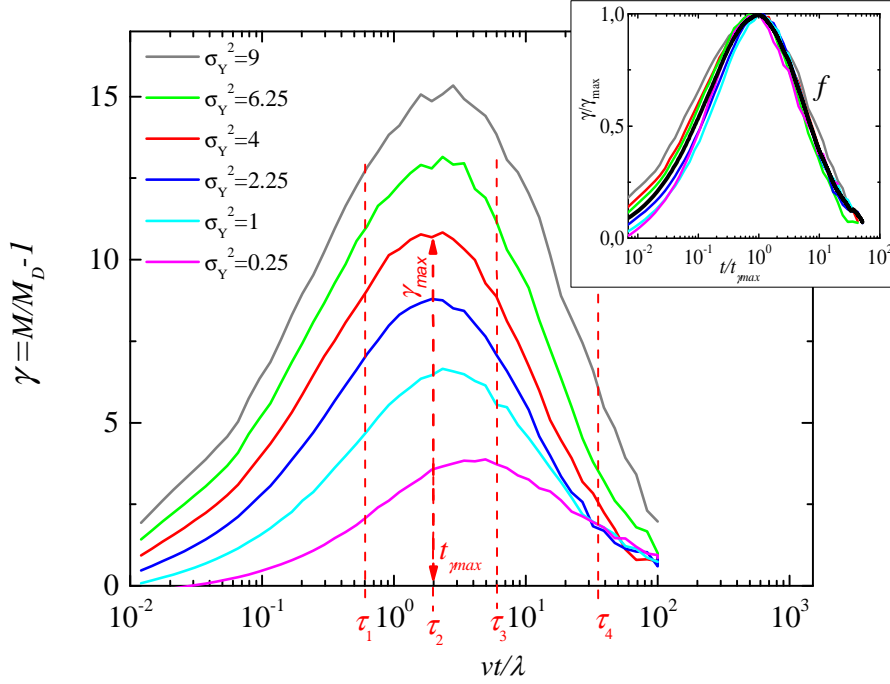
3 Table 1: Values of the maximum deviation to the dispersive mixing regime γ_{\max} for MRMT
4 models with a power-law exponent of the rate distribution $m=2.25$ and $\Delta L_0 / \alpha_{LA} = 0.075$.

5

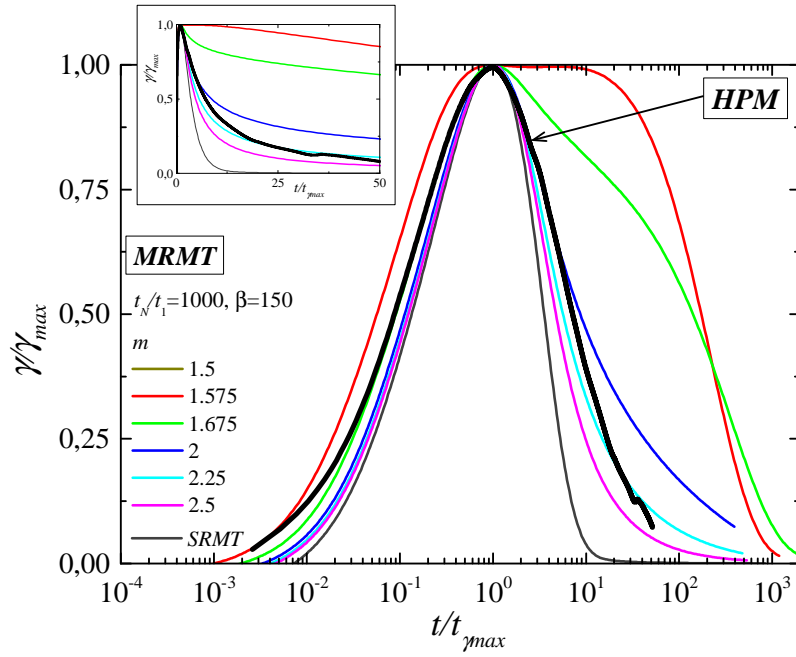


6

7 Figure 1: Concentration fields normalized by their maximal value $c(\mathbf{x},t)/\max(c(\mathbf{x},t))$ and their
 8 related Gaussian profile concentrations $c_D(\mathbf{x},t)/\max(c(\mathbf{x},t))$ in the bar over them at the four
 9 evolving times indicated on Figure 2. In this case, the time at which the non-dispersive
 10 mixing reaches its maximum $t_{\gamma_{\max}}$ is of the same order of the advection time.



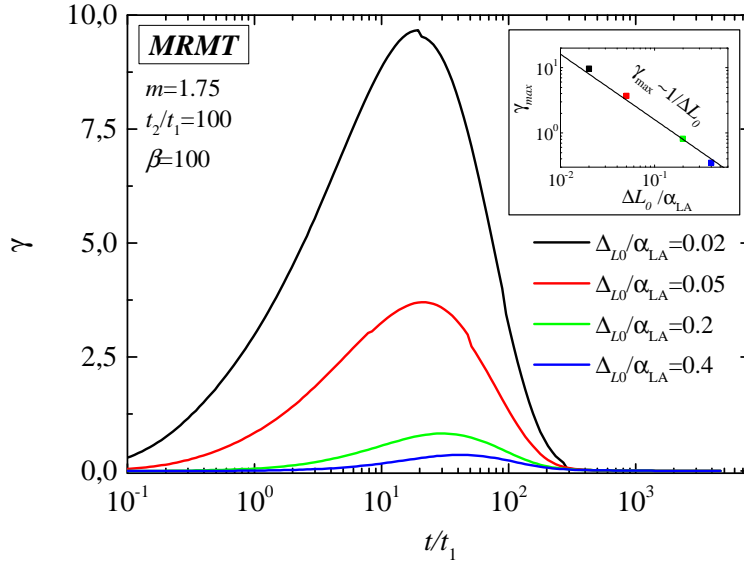
1
2 Figure 2: Time evolution of the deviation from dispersive mixing $\chi(t)$ defined by equation
3 (12) in HPM for evolving log-K variances, σ_Y^2 , under a small width injection window
4 ($\Delta L_0/\alpha_{LA} = 0.075$), flux weighted injection conditions and $Pe=100$ (adapted from *de Dreuzy*
5 *et al.* [2012]). The similarity of function shapes is highlighted in the insert by the scaling
6 function f of equation (16) where the thick black line is the average of the displayed functions.
7 Note that the time of maximum deviation, $t_{\gamma_{max}}$, is hardly affected by σ_Y^2 and falls around the
8 characteristic advection time λ/ν . The four dashed lines indicate the times displayed in Figure
9 1.
10



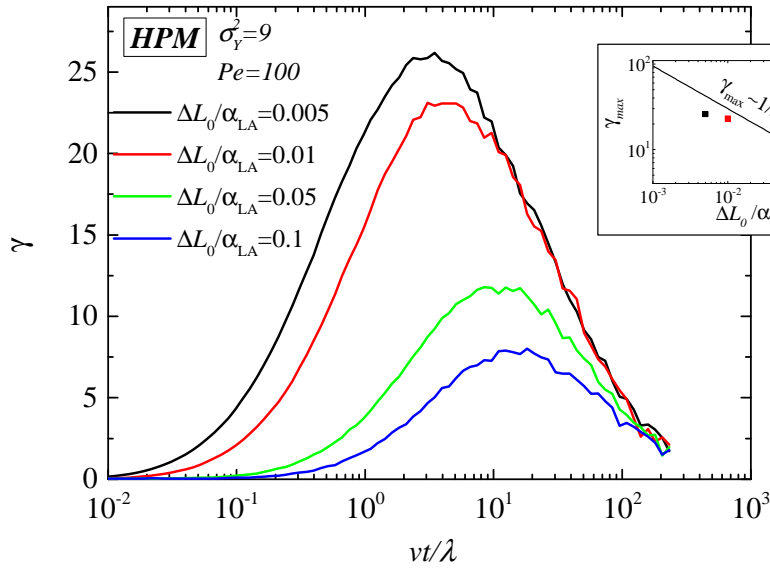
1

2 Figure 3: Comparison of γ shapes (f scaling functions defined in (16)) for HPM and MRMT
 3 simulations with slopes of the power-law distributions of MRMT transfer rates, m , between
 4 1.575 and 2.5. HPM is represented by the broad black curve obtained from the insert of
 5 Figure 2. The insert displays the same curves in arithmetic scale.

(a)



(b)



2 Figure 4: Dependence of the deviation from dispersive function γ on the injection width
 3 $\Delta L_0/\alpha_{LA}$ for (a) MRMT and (b) HPM models. Insert shows the dependence of γ_{\max} on
 4 $\Delta L_0/\alpha_{LA}$.